SUPPLEMENTARY FIGURE LEGENDS

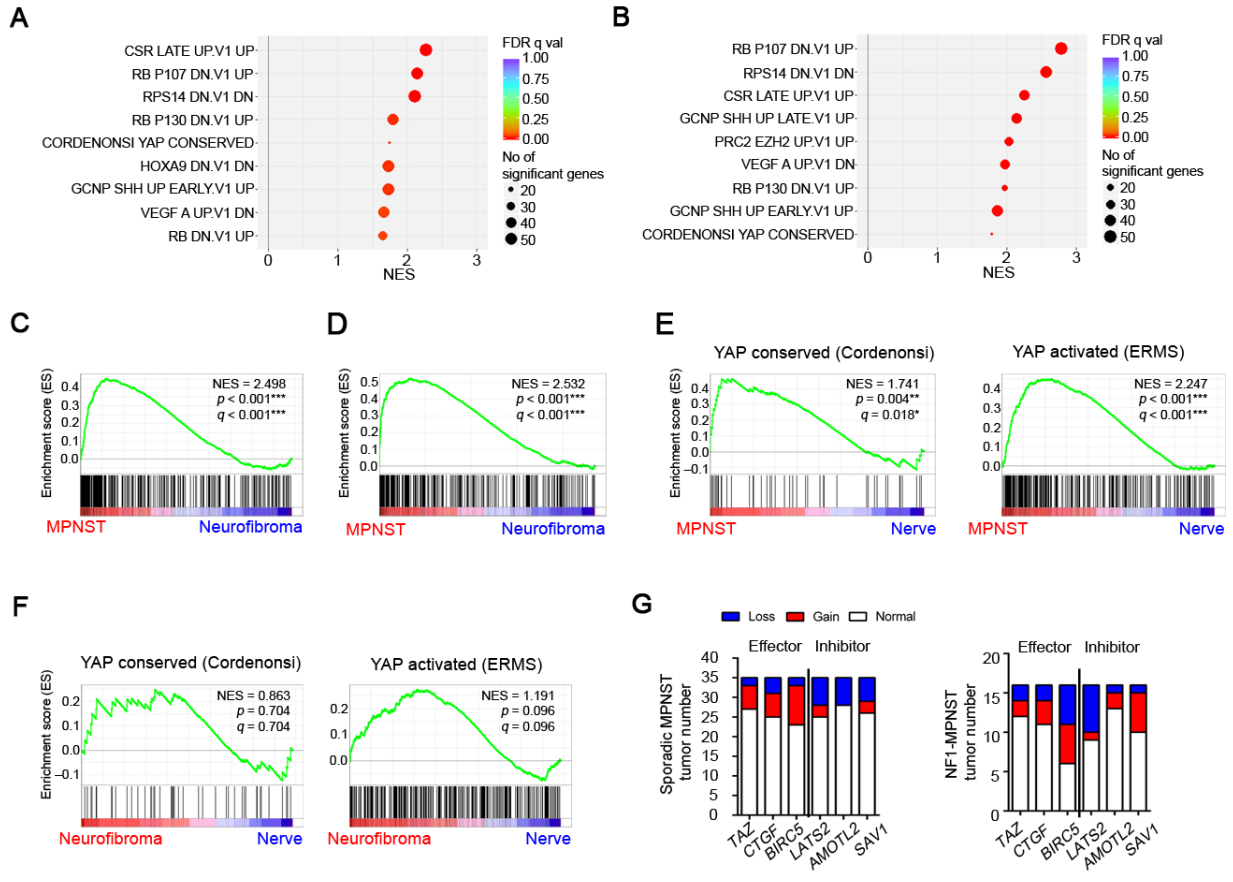

Figure S1. Related to Figure 1. Elevated HIPPO-TAZ/YAP signature in human MPNSTs, but not in neurofibromas.

(A) GSEA enrichment analysis of microarray expression data Jessen_cohort (GSE41747) (Jessen et al., 2013) comparing MPNST (n = 6) and normal nerves (n = 3) for MSigDB C6 oncogenic signatures. Top 9 gene sets up-regulated in MPNST with FDR q values < 0.03 are plotted as a function of normalized enrichment scores (NES). Circle size is proportional to the number of significant genes defined here as the number of genes represented in the leading edge subset, i.e. the subset of members within a gene set that shows statistically significant, concordant differences between two biological states and contribute most to the NES. Circle colors represent FDR q values.

(B) GSEA enrichment analysis of microarray expression data Kolberg_cohort (GSE66743) (Kolberg et al., 2015) comparing MPNST (n = 30) and neurofibroma (n = 8) for MSigDB C6 oncogenic signatures. (Jessen et al., 2013). Top 9 gene sets up-regulated in MPNST are plotted as a function of normalized enrichment scores (NES; see A above).

(C) GSEA enrichment plots show the comparison of normalized gene expression in human MPNSTs (n = 6) and neurofibromas (n = 26) from Jessen_cohort (GSE41747) for YAP-ERMS activated signature.
(D) GSEA enrichment plots show the comparison of normalized gene expression in human MPNSTs (n = 30) and neurofibromas (n = 8) from Kolberg_cohort (GSE66743) for YAP-ERMS activated signature.
(E) GSEA enrichment plots show the comparison of normalized gene expression in human MPNST (n = 6) and nerves (n = 3) from Jessen_cohort (GSE41747) for YAP conserved signature (left) and YAP-ERMS activated signature (right).
(F) GSEA enrichment plots show the comparison of normalized gene expression in human neurofibromas (n = 26) and nerves (n = 3) from Jessen_cohort (GSE41747) for YAP conserved signature (left) and YAP-ERMS activated signature (right).
(G) Copy number analysis of core HIPPO signaling genes in 35 sporadic MPNST patients (left) and 16 NF1-MPNST patients (Yang et al., 2011) reveals copy number alterations in selected HIPPO pathway gene loci.

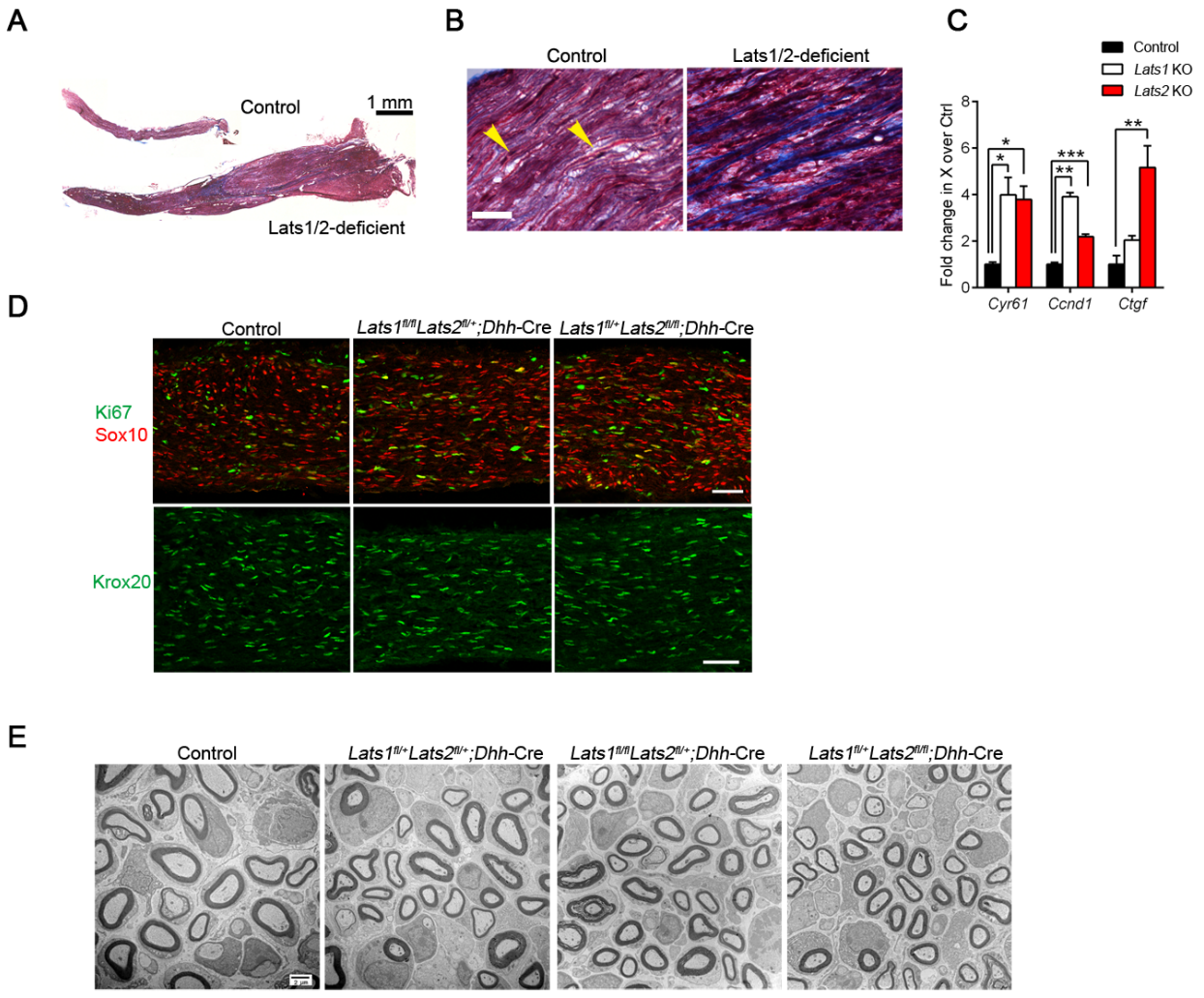

Figure S2. Related to Figure 2. Normal SC development and myelination in Lats1/2-deficient peripheral nerves during early postnatal stages

(A-B) Masson's trichrome-stained longitudinal sciatic nerve sections of control and Lats1/2-deficient mice at 3 months showing enlarged nerve size and an increase in cell number and abundant collagen (blue) in Lats1/2-deficient nerves. Arrowheads: cell nuclei. Scale bars, 1 mm in A; 20 μm in B.

(C) qRT-PCR analysis of expression of selected HIPPO-TAZ/YAP target genes between control (n = 3), *Lats1* KO (n = 4-5) and *Lats2* KO SNs (n = 4-5) at 3 months. Data are presented as mean ± SEM (*p < 0.05; **p < 0.01; ***p < 0.001; One-way ANOVA with Tukey's multiple comparisons test).

(D) Immunofluorescence labeling for Ki67, Sox10 or Krox20 in longitudinal SN sections from control, *Lats1*$^{fl/fl}$*Lats2*$^{fl/+}$*;Dhh*-Cre and *Lats1*$^{fl/+}$*Lats2*$^{fl/fl}$*;Dhh*-Cre mice at P7, when the majority of SCs are undergoing differentiation. Scale bars, 50 μm.

(E) EM images show sciatic nerve ultrastructure in control (*Lats1*$^{fl/fl}$*Lats2*$^{fl/fl}$), *Lats1*$^{fl/+}$*Lats2*$^{fl/+}$*; Dhh*-Cre, *Lats1*$^{fl/fl}$*Lats2*$^{fl/+}$*;Dhh*-Cre and *Lats1*$^{fl/+}$*Lats2*$^{fl/fl}$*;Dhh*-Cre mice at P7. Scale bars, 2 μm.

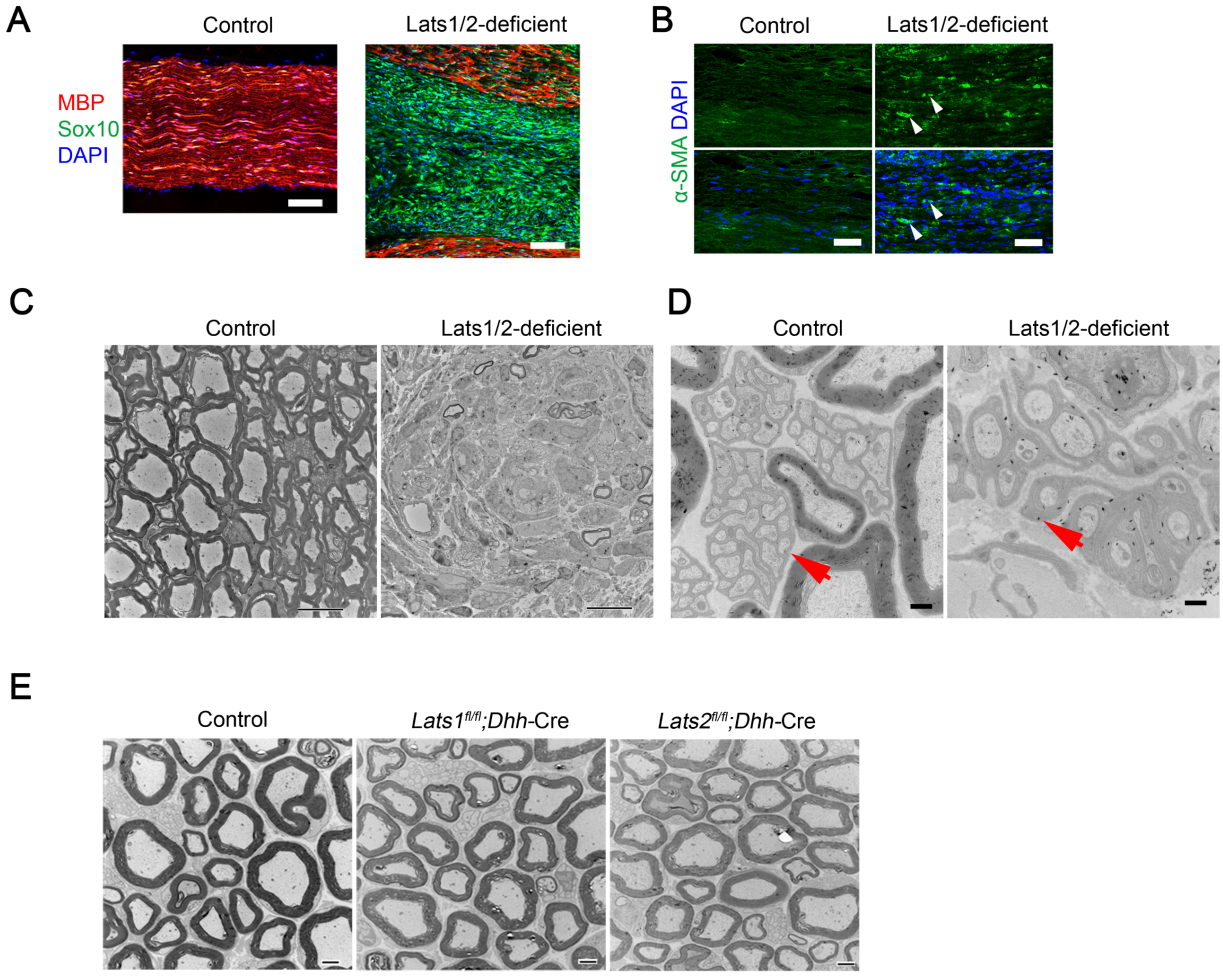

Figure S3. Related to Figure 2. Myelin sheath loss and remark bundle dissociation in Lats1/2-deficient sciatic nerves

(A) Immunofluorescence co-labeling for MBP (red) and Sox10 (green) in longitudinal SN sections of control and Lats1/2-deficient mice at 2.5 months old. DAPI labels cell nuclei. Scale bars, 100 μm.

(B) Immunofluorescence labeling for α-SMA^{+} fibroblasts (green) in longitudinal SN sections of control and Lats1/2-deficient mice at 4 months old. DAPI labels cell nuclei. White arrowheads denote examples of α-SMA^{+} fibroblasts present in mutant nerves. Scale bars, 50 μm.

(C,D) EM analysis of control and Lats1/2-deficient SNs at 2.5 months. Lats1/2-deficient SNs exhibited the loss of myelin sheaths (C) and dissociated axons from Remak bundles (D, arrowheads). Scale bars in C, 2 μm; D, 500 nm.

(E) EM images show fully myelinated axons in sciatic nerve cross-sections from *Lats1* or *Lats2* single mutant (*Lats1*$^{fl/fl}$*;Dhh*-Cre or *Lats2*$^{fl/fl}$*;Dhh*-Cre) mice that are indistinguishable from control nerves at 2.5 months old. Scale bar, 2 μm.

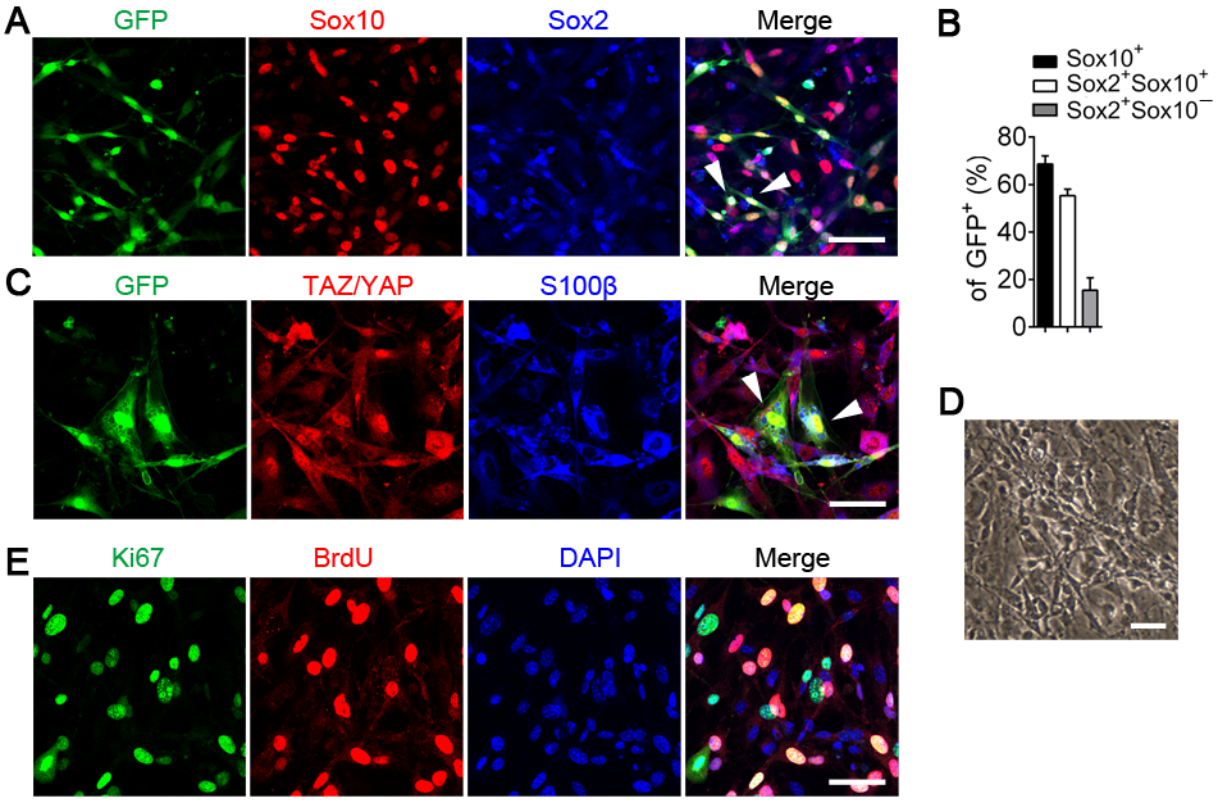

Figure S4. Related to Figure 3. Lineage analysis of Lats1/2-deficient tumor cells confirms SC origin and elevated TAZ/YAP activity

(A) Characterization of GFP^+ cells dissociated from Lats1/2-deficient;$ccGFP^{fl/+}$ paraspinal tumors by immunofluorescence labeling for SC lineage marker, Sox10 (red) and progenitor marker, Sox2 (blue). White arrowheads show examples of triple-labeled $Sox10^+$ $Sox2^+$ GFP^+ cells. Scale bar, 50 µm.

(B) Quantification of the proportions of $Sox10^+$, $Sox2^+$ $Sox10^+$ and $Sox2^+$ $Sox10^-$ cells among GFP^+ cells. Data are presented as mean ± SEM; n = 5 independent cultures.

(C) Immunolabeling for TAZ/YAP (red) and S100β (blue) in GFP^+ cells dissociated from Lats1/2-deficient;$ccGFP^{fl/+}$ paraspinal tumors. White arrowheads show examples of triple-labeled $S100\beta^+$ TAZ/YAP^+ GFP^+ cells. Scale bar, 50 µm.

(D) A brightfield image shows the spindle-shaped morphology of dissociated Lats1/2-deficient tumor cells with enlarged nuclei. Scale bar, 50 µm.

(E) Immunofluorescence labeling for $BrdU^+$ (red; 4-hr pulse) and $Ki67^+$ (green) in tumor cells dissociated from Lats1/2-deficient paraspinal tumors. DAPI labels cell nuclei. Scale bar, 50 µm.

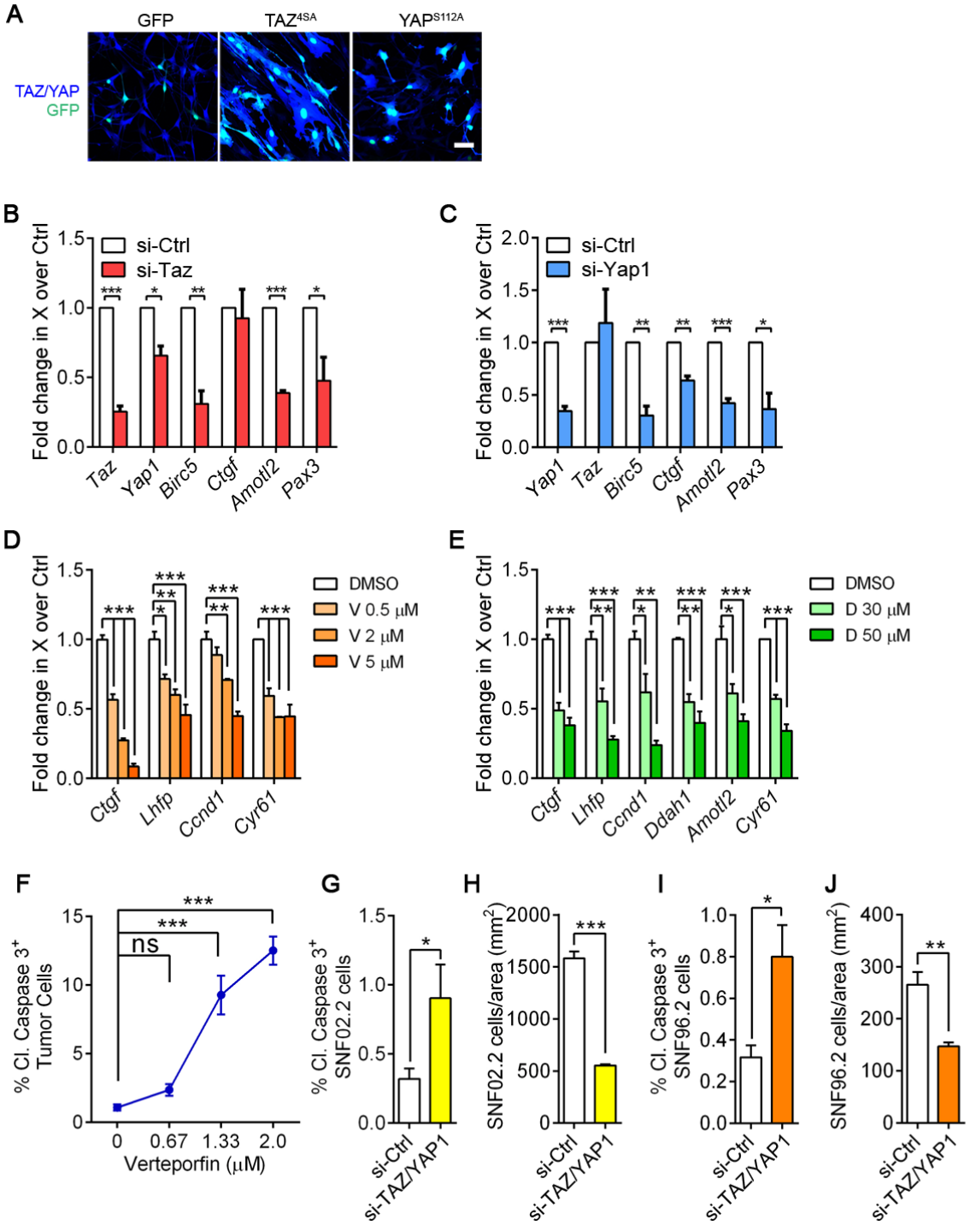

Figure S5. Related to Figure 4. Inactivation of TAZ/YAP effectively downregulates HIPPO target genes and reduces SC proliferation and increases apoptosis in Lats1/2-deficient tumor and human MPNST cells.

(A) Immunostaining of TAZ/YAP in rat SCs transfected with vectors expressing GFP, TAZ^{4SA} or YAP^{S112A} for 48 hr. Scale bars, 50 μm.

(B-C) qRT-PCR analyses of mRNA expression of HIPPO effectors, *Taz*, *Yap* and selected HIPPO-TAZ/YAP target genes between si-control (si-Ctrl) and si-Taz (B) or si-Yap1 (C) knockdown Lats1/2-deficient paraspinal tumor cells. Data are presented as mean ± SEM (*p < 0.05, **p < 0.01, ***p < 0.001; One-way ANOVA with Tukey's multiple comparisons test.

(D-E) qRT-PCR analysis of selected HIPPO-TAZ/YAP target gene expression between DMSO-treated and verteporfin (V)-treated (in D) or dobutamine (D)-treated (in E) Lats1/2-deficient paraspinal tumor cells for 24 hours *in vitro*. Data are presented as mean ± SEM (*p < 0.05, **p < 0.01, ***p < 0.001; One-way ANOVA with Tukey's multiple comparisons test).

(F) Quantification of cleaved caspase 3^+ Lats1/2-deficient paraspinal tumor cells treated with increasing concentrations of verteporfin. Data are presented as mean ± SEM (***p < 0.001; One-way ANOVA with Tukey's multiple comparisons test).

(G) Quantification of cleaved caspase 3^+ human MPNST SNF02.2 cells with combined si-TAZ and si-YAP1 knockdown after 72 hr *in vitro*. Data are presented as mean ± SEM (*p < 0.05; Student's t-test).

(H) Quantification of cell density of human MPNST SNF02.2 cells with combined si-TAZ and si-YAP1 knockdown. Data are presented as mean ± SEM (***p < 0.001; Student's t-test).

(I) Quantification of cleaved caspase 3^+ human MPNST SNF96.2 cells with combined si-TAZ and si-YAP1 knockdown after 72 hr *in vitro*. Data are presented as mean ± SEM (*p < 0.05; Student's t-test).

(J) Quantification of cell density of human MPNST SNF96.2 cells with combined si-TAZ and si-YAP1 knockdown. Data are presented as mean ± SEM (**p < 0.01; Student's t-test).

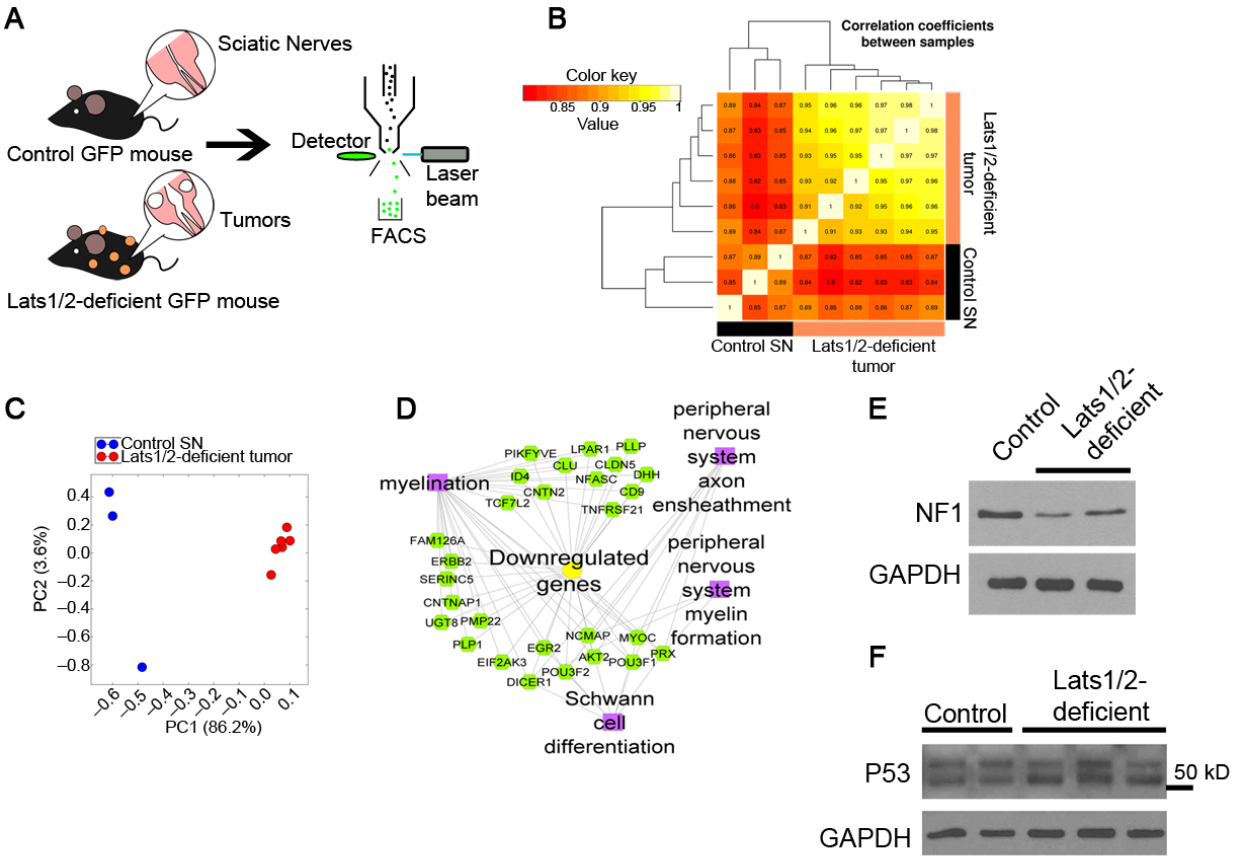

Figure S6. Related to Figure 6. Distinct transcriptome profiles between GFP$^+$ SCs from Lats1/2-deficient and control mice.

(A) Diagram shows isolation of GFP$^+$ SC lineage cells by fluorescence-activated cell sorting (FACS) from dissociated control (*ccGFP$^{fl/+}$;Dhh*-Cre, *Lats1$^{fl/+}$;ccGFP$^{fl/+}$;Dhh*-Cre or *Lats2$^{fl/+}$; ccGFP$^{fl/+}$;Dhh*-Cre or *Lats1$^{fl/+}$Lats2$^{fl/+}$;ccGFP$^{fl/+}$;Dhh*-Cre) SNs and Lats1/2-deficient paraspinal or nerve-associated tumors.

(B) Hierarchical clustering of Pearson correlations of DESeq2 normalized counts for the *in vivo* RNA-seq libraries between control GFP$^+$ SCs and Lats1/2-deficient GFP$^+$ SCs. Color represent Pearson correlation coefficient and values are displayed on their corresponding heatmap tiles.

(C) PCA analysis shows a strong correlation between Lats1/2-deficient tumor samples that are distinctly clustered from control GFP$^+$ SCs.

(D) ToppCluster analysis shows functional networks among the genes and their associated biological processes downregulated in Lats1/2-deficient GFP$^+$ SCs.

(E) Immunoblots show reduction in NF1 protein levels in Lats1/2-deficient sciatic nerves compared with normal adult mouse nerves. GAPDH is a loading control.

(F) Immunoblots show modestly altered P53 protein levels in Lats1/2-deficient sciatic nerves compared with normal adult mouse nerves. GAPDH is a loading control.

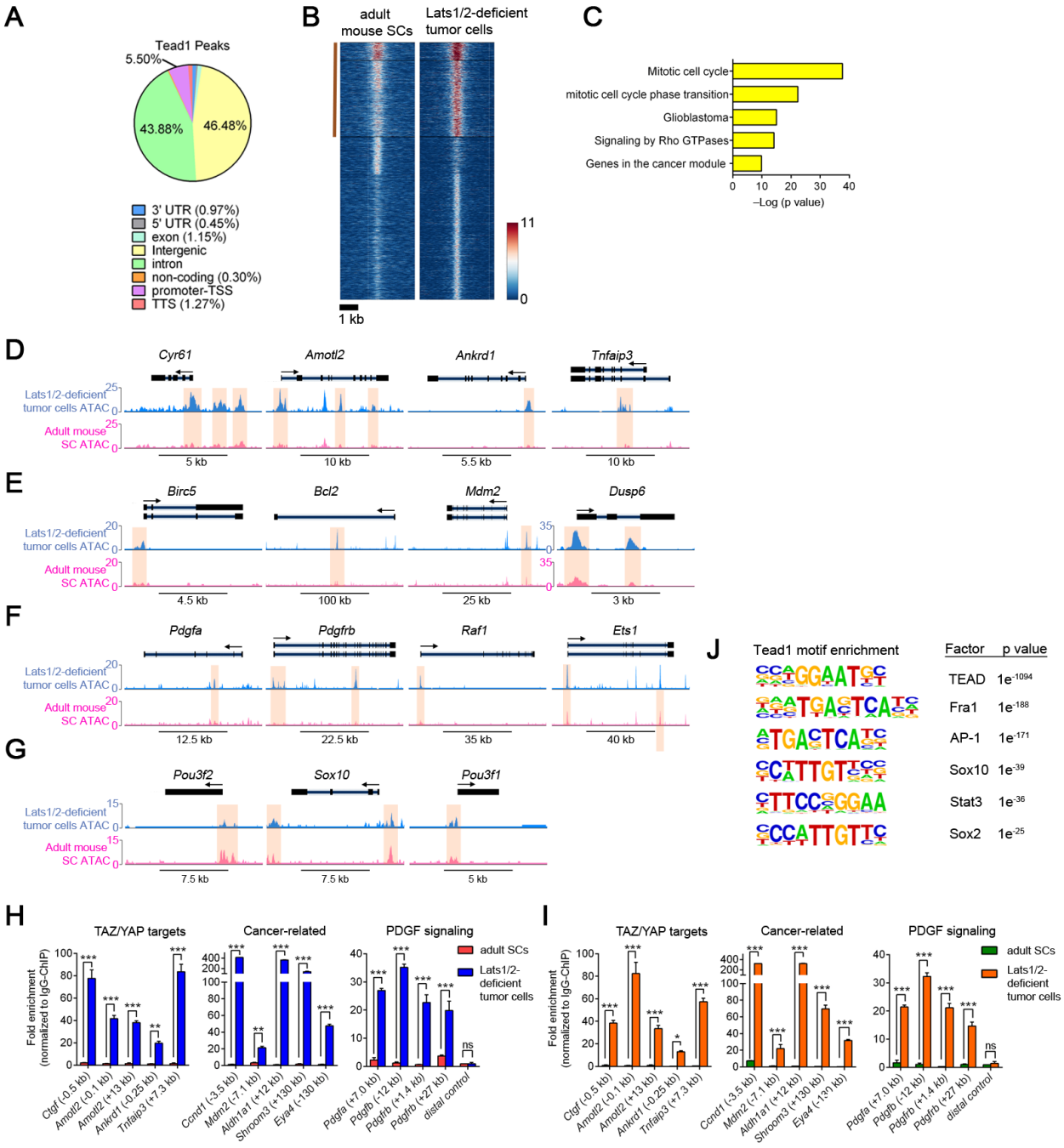

Figure S7. Related to Figure 7. ATAC-sequencing reveals open chromatin at cancer-related gene loci in Lats1/2-deficient tumor cells

(A) Pie chart of the genomic location distribution of transcription factor TEAD1.

(B) ATAC-seq density heatmaps of adult mouse SCs (mSCs) and Lats1/2-deficient tumor cells within ± 2 kb around the peak center. Brown line denotes peaks that show more accessible chromatin in Lats1/2-deficient tumor cells than in mSCs.

(C) GO analysis of genes, indicated by the brown line in B, whose loci are more accessible in Lats1/2-deficient tumor cells compared with mSCs.
(D-E) ATAC-seq profiles on HIPPO-TAZ/YAP target loci (D) or oncogene loci (E) in Lats1/2-deficient tumor cells compared with normal adult mouse SCs. Shaded areas: ATAC-seq peaks.
(F) ATAC-seq profiles on selected gene loci in the PDGF pathway in Lats1/2-deficient tumor cells compared with adult mouse SCs. Shaded areas: ATAC-seq peaks.
(G)ATAC-seq profiles on selected gene loci in SC identity and differentiation in Lats1/2-deficient tumor cells compared with adult mouse SCs. Shaded areas: ATAC-seq peaks.
(H-I) TEAD1 (H) or TAZ (I) occupancy by ChIP–PCR in Lats1/2-deficient tumor cells compared with adult mouse SCs at the regulatory elements with TEAD1 consensus binding sites (GGAAT) of TAZ/YAP target genes, cancer-related genes and PDGF signaling genes. A distal gene region without TEAD1 binding sites was an internal control. Fold enrichment was normalized to IgG-ChIP negative control. Data are mean ± SEM; *$p < 0.05$, **$p < 0.01$, ***$p < 0.001$; $n = 3$ independent experiments; Two-way ANOVA with Sidak's multiple comparisons test.
(J) HOMER analysis of the most highly represented known motifs in the TEAD1 cistrome in Lats1/2-deficient tumor cells.

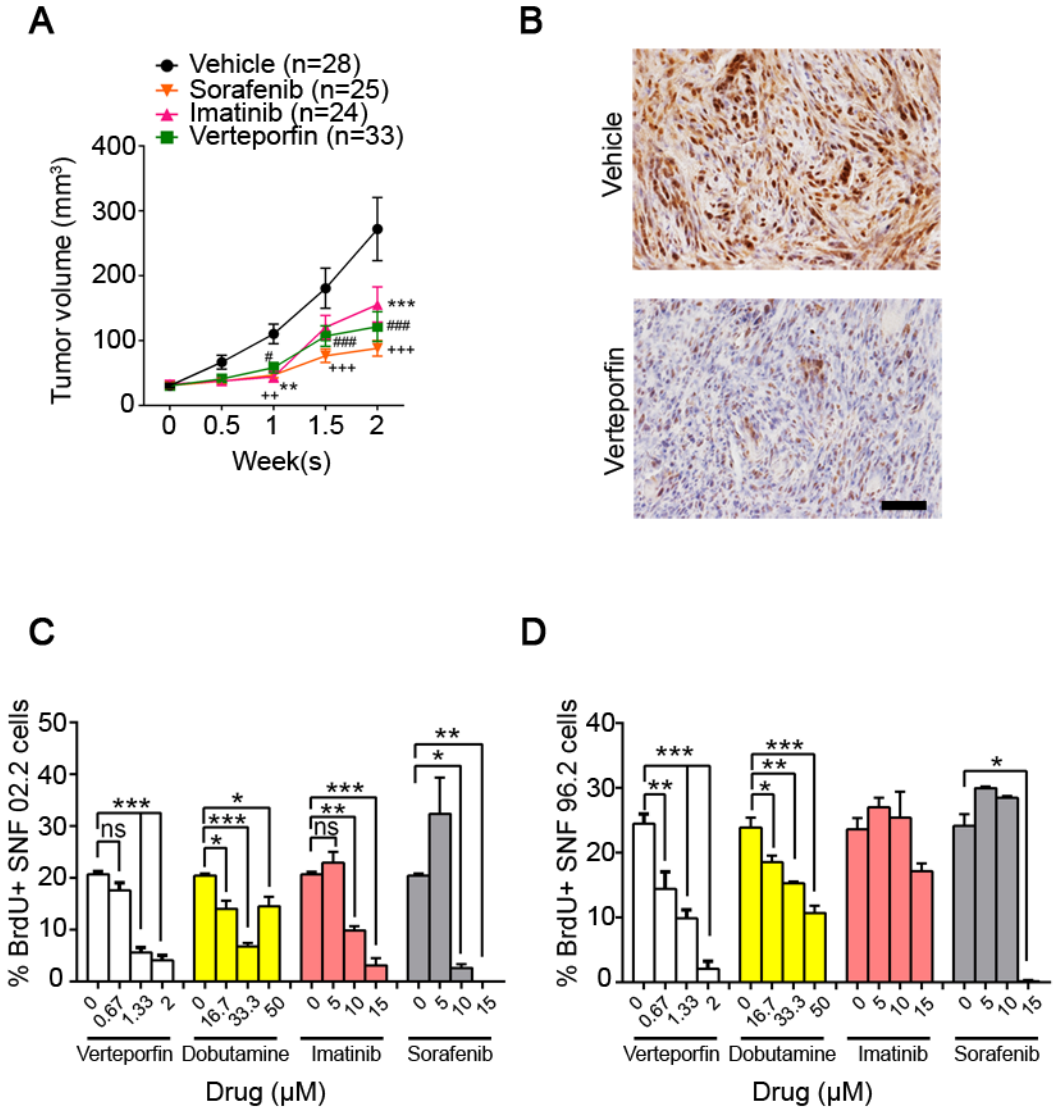

Figure S8. Related to Figure 8. Pharmacological inhibition of TAZ/YAP and PDGF signaling activity impedes Lats1/2-deficient tumor and human MPNST cell line growth.

(A) Tumor growth in athymic nude mice implanted subcutaneously into the flanks with Lats1/2-deficient tumor cell allografts (1×10^5 cells) under daily treatment with 50 mg/kg verteporfin (n = 33 tumors), 40 mg/kg sorafenib (n = 25 tumors) or 50 mg/kg imatinib (n = 24 tumors) as compared to vehicle (n = 28 tumors). Data are presented as mean ± SEM ($^{\#}p < 0.05$; **, $^{\#\#}p < 0.01$; $^{+++}$, $^{\#\#\#}$, ***$p < 0.001$; Two-way ANOVA with Tukey's multiple comparisons test).

(B) DAB immunostaining for TAZ/YAP shows dramatically reduced TAZ/YAP immunoreactivity in allograft tumors from nude mice treated with verteporfin at reduced doses (10 mg/kg) for a 28-day treatment period, compared with tumors from vehicle-treated mice. Scale bars, 50 μm.

(C) Quantification of proliferation by BrdU incorporation (12 hr pulse) in human MPNST SNF02.2 cells treated with TAZ/YAP inhibitors or PDGF signaling inhibitors at the concentrations

indicated. Data are presented as mean ± SEM (n = 3 independent experiments; *p < 0.05, **p < 0.01, ***p < 0.001; One-way ANOVA with Tukey's multiple comparisons test).

(D) Quantification of proliferation by BrdU incorporation (12 hr pulse) in human MPNST SNF96.2 cells treated with TAZ/YAP inhibitors or PDGF signaling inhibitors at the concentrations indicated. Data are presented as mean ± SEM (n = 3 independent experiments; *p < 0.05, **p < 0.01, ***p < 0.001; One-way ANOVA with Tukey's multiple comparisons test).

Table S1, Related to STAR Methods: Oligonucleotides used in the study		
ChIP PCR assay primers		
REAGENT	SOURCE	IDENTIFIER
Mouse *Ctgf* -0.5 kb Forward	Integrated DNA Technologies	TTTCAGACGGAGGAATGTGG
Mouse *Ctgf* -0.5 kb Reverse	Integrated DNA Technologies	TGAATGGAGTCCTACACAAACA
Mouse *Ankrd1* -0.25 kb Forward	Integrated DNA Technologies	TCCCGATACGTGGGATGA
Mouse *Ankrd1* -0.25kb Reverse	Integrated DNA Technologies	CGTATGCGAATCAGGAAGAAATG
Mouse *Amotl2* -0.1 kb Forward	Integrated DNA Technologies	GAGGTTATTTGTGGTTCGCTTTG
Mouse *Amotl2* -0.1 kb Reverse	Integrated DNA Technologies	GCCGATGATCTGCTTGCT
Mouse *Amotl2* +13 kb Forward	Integrated DNA Technologies	ATTTGGAAGAGCCCAGAAAGG
Mouse *Amotl2* +13 kb Reverse	Integrated DNA Technologies	AGGGTTAGAAGCAGGCTGTA
Mouse *Ccnd1* -3.5 kb Forward	Integrated DNA Technologies	GCGTCCAAGGTTTACGGTAA
Mouse *Ccnd1* -3.5 kb Reverse	Integrated DNA Technologies	TAGCCTCCGCGGTCCCACAAAC
Mouse *Eya4* -130 kb Forward	Integrated DNA Technologies	CACAAGCATCCAGTTGAGAATG
Mouse *Eya4* -130 kb Reverse	Integrated DNA Technologies	TGTGAGCTCTGTGTTTAGACTT
Mouse *Shroom3* -130 kb Forward	Integrated DNA Technologies	GGTGCTGTCTCTGAAGGTATG
Mouse *Shroom3*-130 kb Reverse	Integrated DNA Technologies	AACAGATGGCCGCAAGAA
Mouse *Pdgfa* +7.0 kb Forward	Integrated DNA Technologies	GGAAACCCTGAAGGCATCT
Mouse *Pdgfa* +7.0 kb Reverse	Integrated DNA Technologies	CACTTAGAGCTCCTTGACTCTG
Mouse *Pdgfb* -12 kb Forward	Integrated DNA Technologies	CTGCCAGCTCTCCATTCC
Mouse *Pdgfb* -12 kb Reverse	Integrated DNA Technologies	AGAATCTTGCTCGGGTTGG

Mouse *Pdgfrb* +1.4 kb Forward	Integrated DNA Technologies	CTTCCAGATGG TCAGATTCCAG
Mouse *Pdgfrb* +1.4 kb Reverse	Integrated DNA Technologies	GGAGAGGGAA ATGATGAGGA AG
Mouse *Pdgfrb* +27 kb Forward	Integrated DNA Technologies	CTCCCATGAGT CACAAGAATG
Mouse *Pdgfrb* + 27 kb Reverse	Integrated DNA Technologies	GGACTAAAGT CCCAATTCAGG
Mouse *Tnfaip3* +7.3 kb Forward	Integrated DNA Technologies	AGCACCCTTAA GGAGACAGA
Mouse *Tnfaip3* +7.3 kb Reverse	Integrated DNA Technologies	GTGTCGTAGCA AAGTCCTGTT
Mouse *Mdm2* -7.1 kb Forward	Integrated DNA Technologies	AGTGGAGGTC TGGAGAGAAA
Mouse *Mdm2* -7.1 kb Reverse	Integrated DNA Technologies	TCACCCTGTCA GCCTAGAA
Mouse *Aldh1a1*+12 kb Forward	Integrated DNA Technologies	GCAAGGGCTT GTTTCATTACC
Mouse *Aldh1a1*+12 kb Reverse	Integrated DNA Technologies	ACCTTCCACTA TGCCATGC
Mouse DistalTead1-ve Forward	Integrated DNA Technologies	ATACCAAATC ACAAGTTGAC ACC
Mouse DistalTead1-ve Reverse	Integrated DNA Technologies	TTGGTAAACTG TCTACTTACTT CCT
siRNA		
Human TAZ-siRNA	Sigma-Aldrich	SASI_Hs01_0012 4477 - GAUGAAUCAG CCUCUGAAU[d T][dT]
Human TAZ-siRNA	Sigma-Aldrich	SASI_Hs01_0012 4479 - GACUUAGGAA CUUUGGAAU[d T][dT]
Human TAZ-siRNA	Sigma-Aldrich	SASI_Hs01_0012 4480 - GACAAACACC CAUGAACAU[d T][dT]

Human YAP1-siRNA	Sigma-Aldrich	SASI_Hs01_00182402 - CACCUAUCACUCUCGAGAU[dT][dT]
Human YAP1-siRNA	Sigma-Aldrich	SASI_Hs01_00182403 - GCUCAUUCCUCUCCAGCUU[dT][dT]
Human YAP1-siRNA	Sigma-Aldrich	SASI_Hs01_00182404 - CUAAGCAUGAGCAGCUACA[dT][dT]
Mouse Taz-siRNA	Sigma-Aldrich	SASI_Mm01_00107363
Mouse Taz-siRNA	Sigma-Aldrich	SASI_Mm01_00107364
Mouse Taz-siRNA	Sigma-Aldrich	SASI_Mm01_00107365
Mouse Yap1-siRNA	Sigma-Aldrich	SASI_Mm01_00022140
Mouse Yap1-siRNA	Sigma-Aldrich	SASI_Mm01_00022141
Mouse Yap1-siRNA	Sigma-Aldrich	SASI_Mm01_00022142